DYNAMICS-BASED STRUCTURAL WEIGHT OPTIMIZATION OF A LARGE-SCALE 3D CONCRETE PRINTER FRAME WITH TIME-DEPENDENT PRINTHEAD DISPLACEMENT CONSTRAINTS

Duc Khoi Trieu[1], Van Binh Phung[2,*], Reynolds Addo-Akoto[3], Hong Nhu To[1]

DOI: https://doi.org/10.57001/huih5804.2026.117

ABSTRACT

This study proposes a dynamics-based structural weight optimization approach for a large-scale gantry-type 3D concrete printer frame, in which time-dependent printhead displacement is explicitly considered as a performance constraint. Unlike conventional methods based on linear static analysis, the proposed framework integrates flexible multibody dynamic simulation into the optimization loop, enabling direct evaluation of inertial effects and structural vibrations on printhead accuracy. An automated computational framework is developed to couple finite element-based modal analysis, flexible multibody dynamics, and global optimization within a unified iterative process. Elastic characteristics extracted from a parametric finite element model are incorporated into a flexible dynamic model to evaluate printhead displacement under realistic operating conditions. A Genetic Algorithm (GA) is employed to iteratively update design variables, minimizing structural mass while satisfying displacement constraints. The results demonstrate a structural weight reduction of 63.09% while maintaining maximum printhead displacement below 1mm, highlighting the effectiveness of the proposed approach for dynamic-constrained design optimization.

Keywords: *3D concrete printer, Flexible multibody dynamics, Structural weight optimization, Time-dependent printhead displacement, Genetic algorithm*

[1]Faculty of Engineering - Power Supply - Environmental Safety, College of Communication and Technology, Vietnam

[2]Faculty of Aerospace Engineering, Le Quy Don Technical University, Vietnam

[3]Department of Aerospace Engineering, Korea Advanced Institute of Science and Technology, Daejeon 34141, South Korea

[*]Email: phungvanbinh@lqdtu.edu.vn

Received: 20/3/2026

Revised: 15/5/2026

Accepted: 25/5/2026

1. INTRODUCTION

Large-scale 3D concrete printing has gained increasing attention as a promising construction technology because of its high level of automation, reduced labor demand, material efficiency, and improved dimensional control [1]. Among the available system configurations [2], Cartesian gantry systems are widely adopted because of their large workspace and structural stability [3]. However, as the printer scale increases, the frame design problem becomes more challenging, as the structure must provide sufficient stiffness to maintain printhead positioning accuracy while also minimizing structural mass to reduce cost, inertia, and energy consumption [4].

Previous studies on gantry-type structures and large-scale 3D concrete printer frames have predominantly employed linear static analysis. Although such approaches are simple and computationally efficient, they cannot adequately capture actual operating conditions involving inertial effects, structural vibration, and dynamic interactions among moving components [5, 6]. Because printhead displacement varies over time and is strongly affected by the flexible dynamic response of the system, optimization based solely on static models may result in designs that are insufficiently reliable in practice. This concern is supported by previous studies on the flexible dynamic analysis of 3D printer frames, which emphasize the need to account for elastic deformation and time-dependent system behavior [7].

To address these limitations, this study proposes an integrated framework that combines finite element modal analysis, flexible multibody dynamics, and genetic algorithm-based optimization [8-10] for the structural

mass optimization of a large-scale gantry-type 3D concrete printer frame. In this framework, modal characteristics extracted from a parametric finite element model are embedded into a flexible multibody dynamic model, and time-dependent printhead displacement is explicitly incorporated as a design constraint. The automated procedure improves computational efficiency and enables repeated simulations within the optimization loop, thereby providing a more realistic and practically relevant methodology for the design optimization of large-scale 3D concrete printer frames and related flexible mechanical systems subjected to dynamic loading. Unlike conventional studies that employ static deflection or frequency-based criteria, the present work introduces time-dependent printhead displacement as a design constraint.

The present study builds upon a series of previous investigations and extends them toward dynamics-based structural optimization of large-scale 3D concrete printer frames. The work reported in [5] established the structural parameterization scheme, design-variable ranges, and preliminary mass optimization of a simplified large-scale 3D concrete printer frame under static loading conditions. Although this study provided an important foundation for subsequent research, the structural configuration considered was relatively simplified and differed from the more realistic gantry-type printer frame investigated in the present work. Subsequently, the study in [11] investigated the realistic printer-frame configuration considered in this research using an ANN-assisted surrogate model for structural optimization based on static-response criteria. More recently, the automated flexible dynamic simulation framework for this printer-frame configuration was developed in [12], enabling the evaluation of time-dependent printhead displacement under realistic operating conditions.

Unlike these previous studies, the present work directly incorporates flexible dynamic simulation into the optimization process, where each candidate design is evaluated based on its time-dependent printhead displacement response. Consequently, the primary novelty of this study lies in the use of flexible dynamic response as an explicit design constraint for structural weight optimization, thereby enabling a more realistic representation of the operating behavior of large-scale 3D concrete printer frames. The main contributions of this study are threefold: (i) the development of a parametric optimization framework that integrates finite element modal analysis and flexible multibody dynamics, (ii) the explicit incorporation of time-dependent printhead displacement as a design constraint, and (iii) the demonstration of substantial structural mass reduction while maintaining dynamic positioning accuracy.

2. MATERIALS AND METHODS

2.1. Development of a flexible dynamic simulation model for a large-scale 3D concrete printer frame

a) Mechanical configuration and finite element model of the 3D concrete printer frame

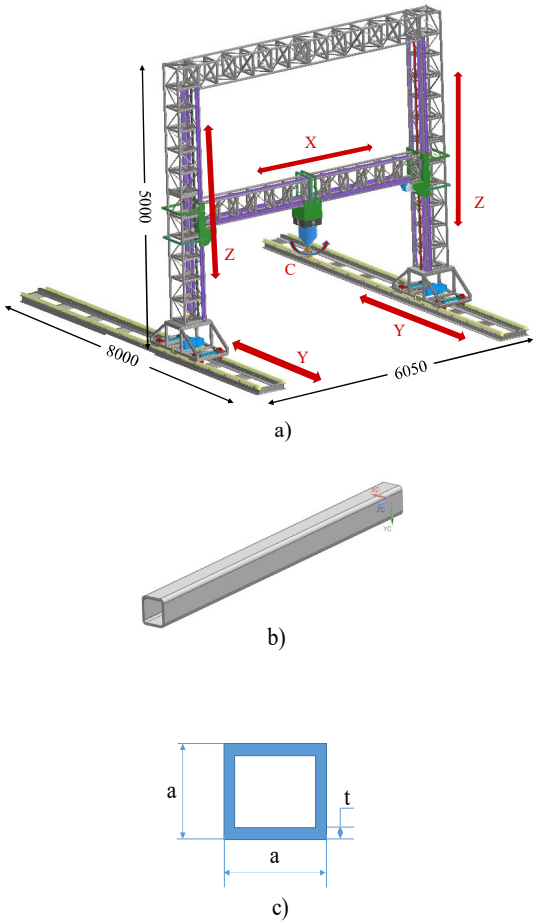

(a) 3D model of the printer; (b) 3D model of hollow steel members; (c) Cross-sectional geometry of the hollow steel section

Figure 1. Preliminary design of the large-scale 3D concrete printer

The 3D concrete printer adopts a large-scale gantry configuration with a printing envelope of 6000×4000×3500 mm, a maximum printhead speed of 20m/min, and allowable positioning errors of ±5mm in the horizontal directions and ±2mm in the vertical direction (Figure 1). The Y-axis gantry and Z-axis subframe are constructed from truss-stiffened square

hollow steel members, with additional stiffeners introduced at critical joints to enhance global stiffness and limit elastic deformation [12]. The entire frame travels along the Y-axis on linear guide rails rigidly mounted on the working platform.

To capture the elastic behavior of the structure, a parametric finite element model is developed in ANSYS APDL. The main geometric variables define the overall frame dimensions as well as the cross-sectional dimensions of the columns, beams, bracing members, and base members of the Y-axis frame. All structural members are modeled using BEAM188 elements based on Timoshenko beam theory. The printhead, motors, and guide rail-related components are represented by equivalent lumped masses using MASS21 elements to capture the inertial characteristics of the moving system [12]. After the interface nodes are defined, modal analysis is performed using the Lanczos algorithm to extract the natural frequencies and mode shapes. These modal characteristics are then used to construct the reduced-order flexible representation for subsequent multibody dynamic simulation. The corresponding finite element model is shown in Figure 2.

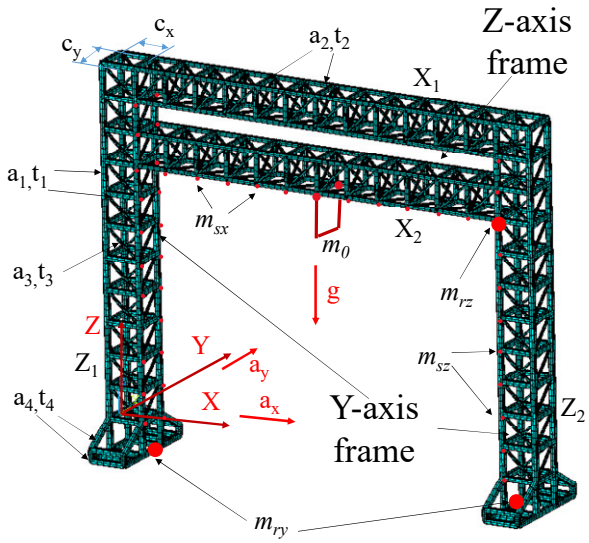

Figure 2. Finite element model of the 3D concrete printer frame

b) Flexible multibody dynamic modeling of the large-scale 3D concrete printer frame

The flexible multibody dynamic model of the printer frame is developed within an integrated framework that combines finite element modal analysis and flexible multibody dynamics. In this framework, a parametric finite element model is established in ANSYS APDL to determine the elastic characteristics of the frame, including its natural frequencies and mode shapes. These modal characteristics are then transferred to the system-level dynamic model in MSC Adams, where flexible bodies replace the corresponding rigid components to capture the effect of structural deformation on printhead motion. The computational process is automated through the integration of ANSYS APDL, MSC Adams, and MATLAB, enabling consistent and efficient parameter updates, simulation execution, and post-processing within the optimization loop [12]. The overall computational workflow is illustrated in Figure 3.

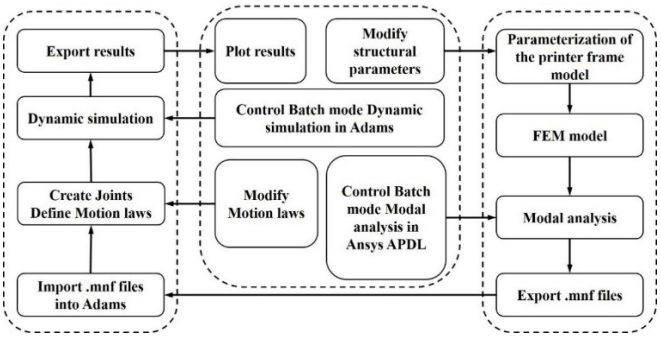

Figure 3. Integrated workflow for automated flexible dynamic simulation of the printer frame

2.2. Mathematical optimization model and optimization procedure for structural weight minimization of a large-scale 3D concrete printer frame

a) Mathematical optimization model

According to the preliminary structural analyses reported in [11], under the most unfavorable operating condition corresponding to the maximum printhead speed and the highest printing position, the maximum stress in the printer frame was approximately 29.1MPa, which is significantly lower than the allowable stress of the structural steel. In contrast, the structural displacement was found to be considerable with respect to the printhead positioning accuracy requirements. Therefore, printhead displacement was identified as the governing design constraint in the present optimization problem. Since the stress levels remained well below the material strength limit throughout the investigated design space, stress constraints were not explicitly included in the optimization model in order to reduce computational complexity and focus on the dynamic accuracy requirements of the printing system.

The structural optimization of the large-scale 3D concrete printer frame is formulated as a constrained optimization problem in which the total structural mass is minimized subject to printhead displacement

constraints. The design vector is defined as $X=\left[C_x, C_y, a_1, t_1, a_2, t_2, a_3, t_3, a_4, t_4\right]^T$, where the lower and upper bounds of each variable are determined based on the preceding parametric study and the manufacturability limits of standard hollow steel sections [5], as summarized in Table 1. Under the investigated operating conditions, the maximum printhead displacements in the X and Y directions are required to remain below 1 mm.

Table 1. Lower and upper bounds of the design variables (mm)

Parameters	Range	Parameters	Range
C_x	460 - 530	C_y	460 - 530
a_1	12 - 75	a_3	12 - 75
t_1	0.7 - 3.5	t_3	0.7 - 3.5
a_2	25 - 75	a_4	12 - 75
t_2	0.7 - 3.5	t_4	0.7 - 3.5

The objective function is the total structural mass of the frame, given by [5]:

$$M=\rho\sum_{i=1}^{n}L_i\left(a_i^2-\left(a_i-2t_i\right)^2\right) \quad (1)$$

where M denotes the total structural mass, ρ = 7850 (kg/m^3) is the density of steel, L_i is the length of the i-th structural member, a_i is the outer side dimension of the square hollow section, and t_i is the wall thickness. The cross-sectional area of the i-th square hollow member is calculated as: $A_i=a_i^2-\left(a_i-2t_i\right)^2$. The displacement constraints are imposed on the maximum printhead displacements in the X and Y directions under the investigated operating conditions. The resulting optimization problem is solved using a genetic algorithm integrated with flexible dynamic simulation, allowing each candidate design to be evaluated directly in terms of both structural mass and maximum printhead displacement.

b) Optimization procedure for structural weight minimization of a large-scale 3D concrete printer frame

The structural mass optimization of the large-scale 3D concrete printer frame is carried out using a genetic algorithm (GA) within an integrated framework that couples parametric structural modeling with flexible dynamic simulation, as illustrated in Figure 4.

In this framework, each individual is represented by a real-valued vector of ten geometric design variables, and its fitness is evaluated based on the structural mass objective and displacement constraints. As a global stochastic optimizer, the GA is well suited to nonlinear and non-convex problems because it does not require gradient information and reduces the risk of convergence to local optima. At each generation, selection, crossover, mutation, and elitism are applied to evolve the population toward improved candidate solutions. For each candidate design, the parametric structural model is automatically updated, the modal characteristics are extracted, and the corresponding flexible multibody dynamic response is evaluated under the prescribed operating conditions [8, 11]. This evaluation cycle is repeated until convergence is achieved or the maximum number of generations is reached. Owing to the fully automated workflow, the proposed procedure enables structural optimization under representative dynamic operating conditions while substantially reducing the time required for each design-evaluation cycle, from approximately 40 - 60 minutes in the manual procedure to about 10 minutes in the automated framework.

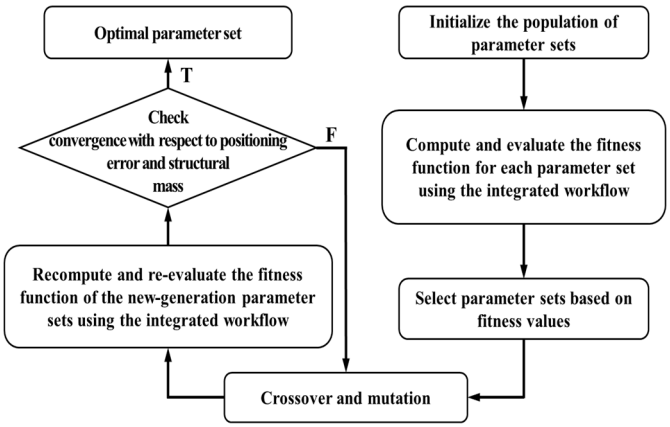

Figure 4. Flowchart of the GA-based structural mass optimization process

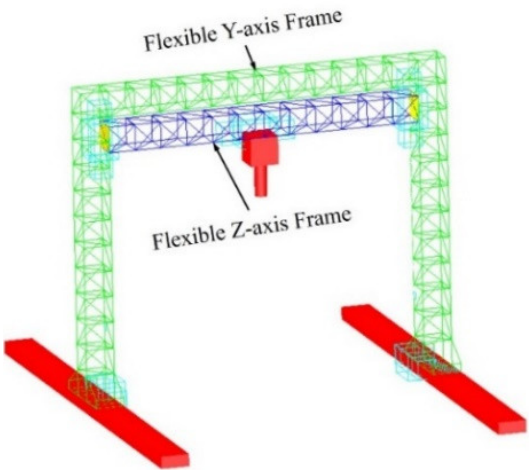

(a) flexible multibody dynamic model

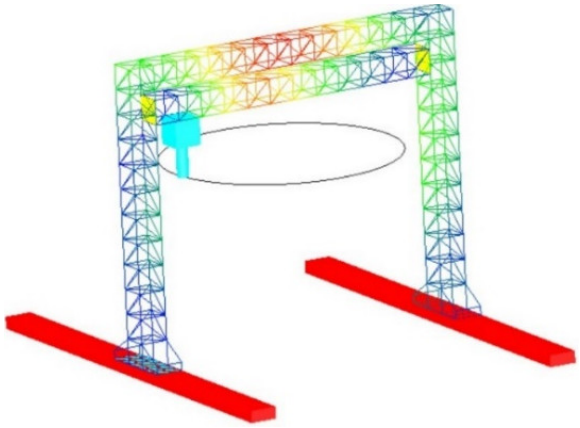

(b) simulated printhead trajectory

Figure 5. Flexible dynamic simulation of the 3D concrete printer

3. RESULTS AND DISCUSSION

3.1. Dependence of printhead displacement on the design parameters

To determine feasible ranges of the design parameters, the printhead displacement is evaluated under a representative operating condition in which the printhead follows a circular trajectory with a radius of 0.5m at the maximum speed of 20m/min on the printing plane at Z = 3m. The corresponding flexible dynamic model and simulated printhead trajectory are shown in Figure 5. This operating condition was selected as a representative unfavorable scenario for the investigated printer. The printhead speed of 20m/min corresponds to the maximum operating speed of the system, while the printing plane at Z = 3m represents an elevated working position where the gantry frame is more susceptible to elastic deformation and vibration. As a result, relatively large printhead displacement can be expected, making this condition suitable for evaluating the proposed optimization framework. In addition, the circular trajectory continuously changes the direction of printhead motion, producing centripetal acceleration and stronger dynamic excitation than simple linear motion. Therefore, this combination of high speed, large printing height, and curved trajectory provides a meaningful condition for evaluating the influence of structural flexibility on printhead accuracy. Nevertheless, the optimized result should be interpreted as directly valid for the investigated operating scenario; further studies with different trajectories, speeds, and printing heights are required to assess the general applicability of the optimized design.

Each simulation is conducted over five motion cycles, with the first two cycles excluded to eliminate transient effects. All cases are executed automatically using the developed integrated framework. Because previous studies have shown that the printhead displacement in the Y direction is dominant, the present analysis focuses on the Y-axis response. As shown in Figure 6, the displacement is influenced primarily by the global geometric parameters C_x and C_y, whereas reductions in the cross-sectional dimensions a_1, a_2, a_3, and a_4 also increase the displacement, although to a lesser extent. In contrast, variations in the wall thicknesses t_1 - t_4 have only a minor influence on printhead displacement, although they directly affect the total structural mass. These results indicate that subsequent structural mass optimization should primarily target the sectional dimensions and wall thicknesses, while the global frame geometry should be carefully controlled. In addition, the automated framework substantially reduces the time required for each simulation case, from approximately 40 - 60 minutes in the manual workflow to about 10 minutes in the automated procedure, thereby demonstrating its efficiency for repeated simulation-based optimization.

3.2. Optimization results and discussion

This section presents the GA-based optimization results obtained using a population of 20 individuals evolved over 25 generations within the integrated flexible dynamic simulation framework. The GA settings were selected by considering both convergence behavior and computational cost. Since each individual requires a complete simulation cycle, including finite element model updating, modal extraction, flexible multibody dynamic simulation, and displacement post-processing, the population size must balance design diversity and simulation effort. A population of 20 individuals was therefore adopted as a practical compromise, while the maximum number of generations was set to 25 to allow sufficient evolution of the population toward a stable solution region. Figures 7(a) and 7(b) show the distribution of individuals with respect to the printhead displacement constraint and the convergence history of the structural mass, respectively.

The results indicate that the population gradually converges toward a feasible solution region satisfying the displacement constraint of 1mm, while the structural mass progressively narrows to a range of approximately 300 - 500kg. The best individual obtained during the optimization process has a mass of 359.67kg. A pronounced mass reduction is observed in the early generations, followed by a slower rate of improvement

and gradual stabilization, which is consistent with a transition from global exploration to local exploitation of promising design regions.

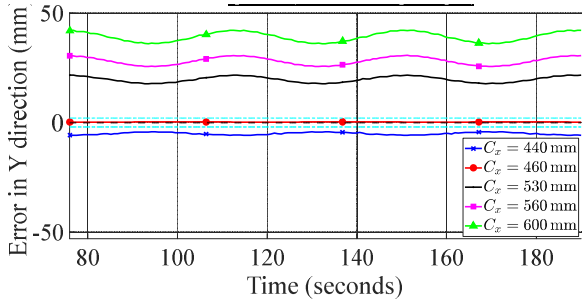

(a) Variation of C_x

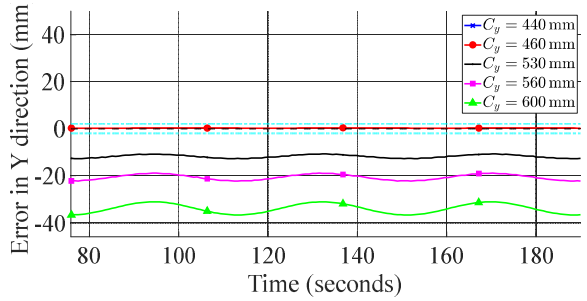

(b) Variation of C_y

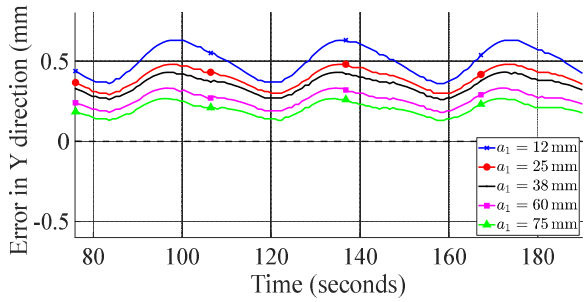

(c) Variation of a_1

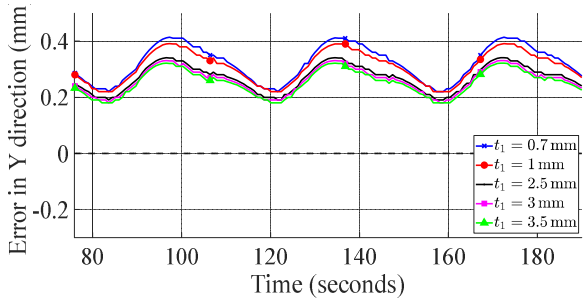

(d) Variation of t_1

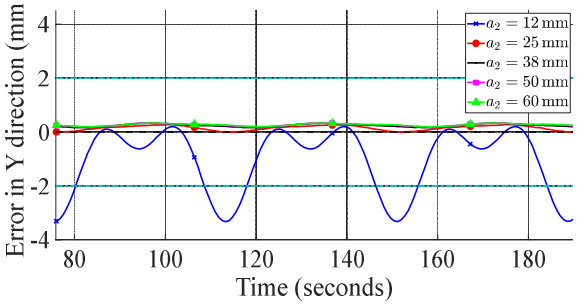

(e) Variation of a_2

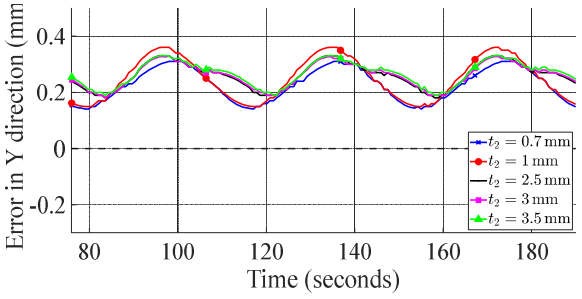

(f) Variation of t_2

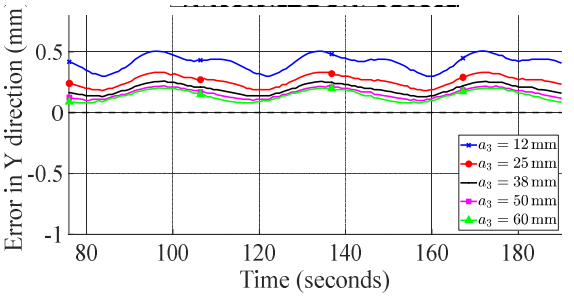

(g) Variation of a_3

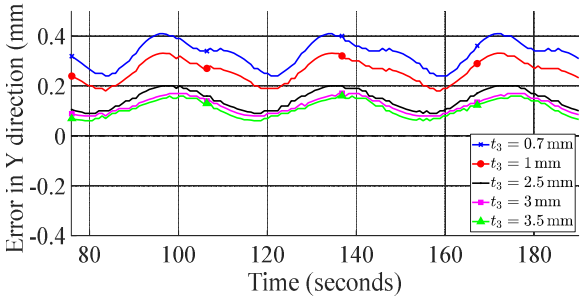

(h) Variation of t_3

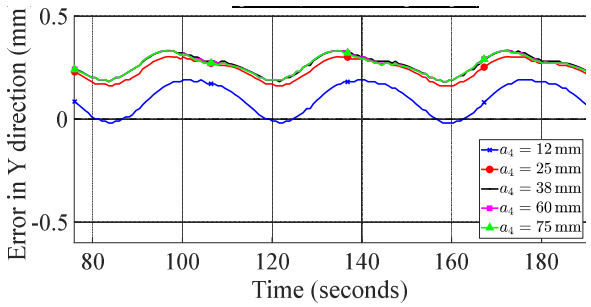

(i) Variation of a_4

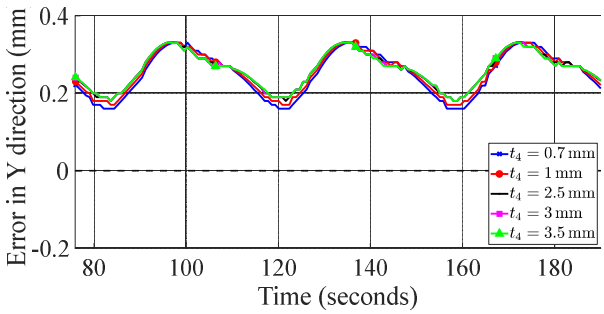

(k) Variation of t_4

Figure 6. Effect of design parameter variations on printhead displacement in the Y direction

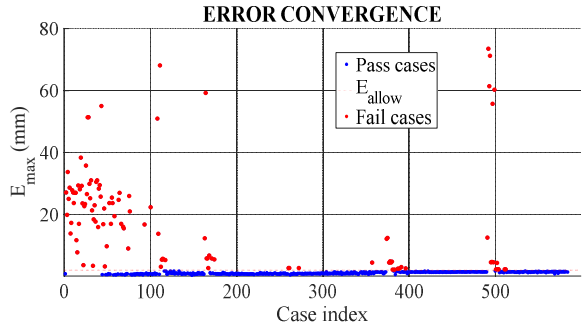

(a) Distribution of individuals with respect to the printhead displacement constraint

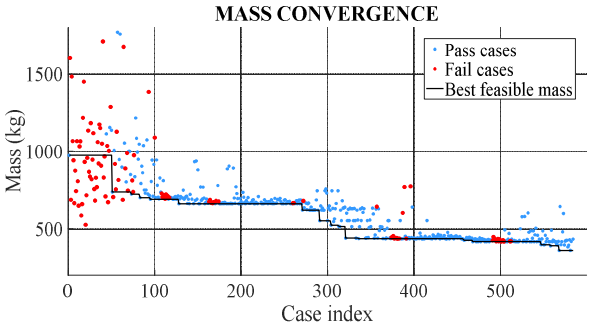

(b) Convergence history of structural mass

Figure 7. GA optimization results

The relative convergence rate, denoted by R_c, is defined as:

$$R_c = \frac{f_{best}^{(t)} - f_{best}^{(t-1)}}{f_{best}^{(t-1)}} \quad (2)$$

where $f_{best}^{(t)}$ and $f_{best}^{(t-1)}$ represent the best fitness values at generations t and (t - 1), respectively. The evolution of the relative convergence rate is shown in Figure 8.

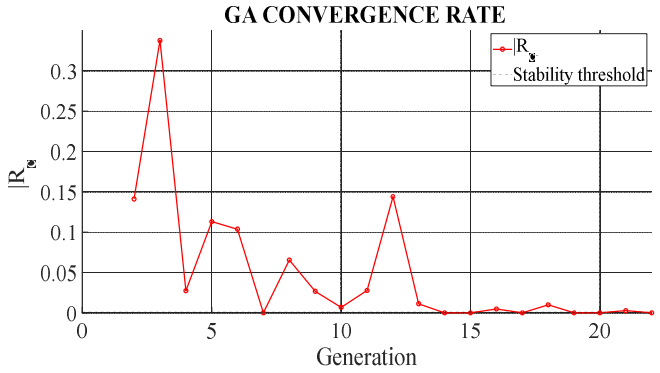

Figure 8. Evolution of the relative convergence rate during the optimization process

Large fluctuations are observed between generations 2 and 12, corresponding to the global search stage, whereas a sharp decrease occurs around generations 13 and 14. From generation 15 onward, the improvement between successive generations becomes negligible, indicating that the algorithm approaches a stable state without clear evidence of premature convergence.

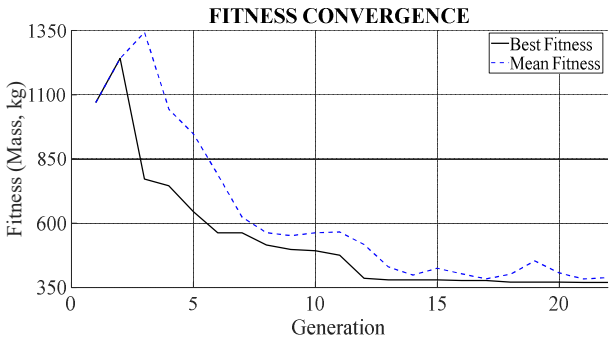

Figure 9. Convergence trends of the best and average fitness values

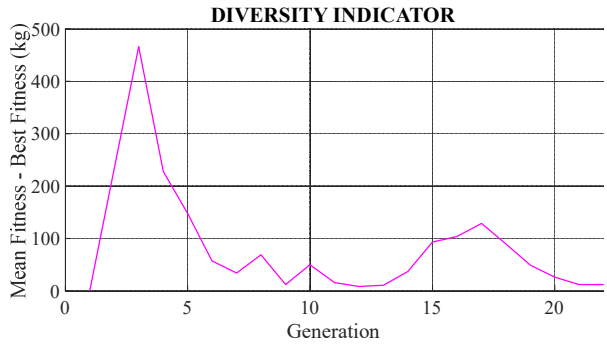

Figure 10. Difference between the best and average fitness values

To further examine the convergence behavior, Figures 9 and 10 compare the evolution of the best and average fitness values and the difference between them over successive generations. The results reveal three characteristic stages: an initial exploration stage with rapid improvement and large fluctuations, an intermediate stage marked by reduced improvement and increasing population homogeneity, and a final stage in which the best and average fitness values become nearly identical, indicating stable convergence of the population. These observations suggest that the GA is able to identify a feasible near-optimal solution satisfying the imposed constraints while maintaining stable convergence behavior throughout the optimization process.

At the 25th generation, the difference between the best and average fitness values becomes relatively small, indicating that the population has approached a stable convergence state. Therefore, extending the optimization beyond 25 generations is expected to provide only marginal improvement while increasing the computational cost. This observation further supports the selection of 25 generations as a suitable stopping limit for the present simulation-based optimization problem.

(a) The printhead displacement in the X direction

(b) The printhead displacement in the Y direction

Figure 11. The printhead displacement of the optimal design in the X and Y directions

The printhead displacement of the optimal design is further verified in Figures 11(a) and 11(b), while Table 2 compares the preliminary and optimal designs. The results show that the displacement remains stable in both directions and below the allowable limit of 1mm, with maximum values of 0.112mm in the X direction and 0.815 mm in the Y direction. Compared with the preliminary design, the structural mass is reduced from 974.50kg to 359.67kg, corresponding to a reduction of 63.09%, while fully satisfying the imposed displacement constraints. The relatively large mass reduction can be explained by the characteristics of the preliminary design. In the early design stage, the frame dimensions were selected based on engineering experience and conservative design assumptions to ensure sufficient stiffness and safety margins. As a result, the initial structure contained a considerable amount of excess material. During the optimization process, the GA simultaneously adjusted the cross-sectional dimensions and wall thicknesses of all structural member groups within the predefined design space, enabling a more efficient redistribution of material throughout the frame. Consequently, a substantial reduction in structural mass was achieved while maintaining the required printhead positioning accuracy.

To further assess the mechanical feasibility of the optimized design, the dynamic characteristics of the frame were also examined. Although the first three natural frequencies of the optimized frame are lower than those of the preliminary design, indicating a reduction in low-order dynamic stiffness, all natural frequencies remain significantly higher than the dominant excitation frequency associated with the investigated operating condition. For the circular trajectory with a radius of 0.5m and a printhead speed of 20 m/min, the fundamental motion frequency is approximately 0.106Hz, whereas the first natural frequency of the optimized frame is 3.972Hz. Therefore, the risk of resonance can be considered negligible under the investigated operating condition.

In addition, preliminary structural analyses reported in [11] showed that the maximum stress of this printer-frame configuration remained well below the allowable stress of the structural steel, even under unfavorable operating conditions. Combined with the displacement verification presented in Figures 11(a) and 11(b) and the modal analysis results, these findings confirm that the optimized design not only satisfies the prescribed positioning-accuracy requirements but also maintains acceptable structural integrity and dynamic performance. Therefore, the proposed optimal design can be considered mechanically feasible for practical large-scale 3D concrete printing applications.

Table 2. Comparison between the preliminary design and the optimal design

Parameter	Preliminary design	Optimal design
C_x (mm)	460	460
C_y (mm)	460	460
$a_1 \times a_1 \times t_1$ (mm)	$60 \times 60 \times 3$	$32.2 \times 32.2 \times 1.41$
$a_2 \times a_2 \times t_2$ (mm)	$50 \times 50 \times 2.5$	$50 \times 50 \times 1.23$
$a_3 \times a_3 \times t_3$ (mm)	$25 \times 25 \times 1$	$17.2 \times 17.2 \times 0.88$
$a_4 \times a_4 \times t_4$ (mm)	$60 \times 60 \times 3$	$15.8 \times 15.8 \times 1.69$
First natural frequency (Hz)	7.0122	3.9720
Second natural frequency (Hz)	9.2059	4.1866
Third natural frequency (Hz)	12.192	8.6368
Maximum printhead displacement in X (mm)	0.066	0.112 (Satisfied)
Maximum printhead displacement in Y (mm)	0.404	0.815 (Satisfied)
Mass (kg)	974.50	359.67
Mass reduction (%)	-	63.09%

4. CONCLUSION

This study proposed a structural weight optimization approach for a large-scale 3D concrete printer frame by

integrating a GA with flexible dynamic simulation within an automated computational framework. The developed methodology enables coupling among finite element–based modal analysis, flexible multibody dynamics, and global stochastic optimization, forming a closed-loop iterative procedure. A flexible dynamic model of the printer frame was established by extracting modal characteristics from the finite element representation and embedding them into the multibody dynamic formulation. The automated workflow ensures data consistency between structural and dynamic analyses while significantly reducing computational time from 40 - 60 minutes to approximately 10 minutes per simulation cycle.

The parametric investigation revealed that the global geometric dimensions of the frame (C_x, C_y) exert a dominant influence on printhead displacement, whereas section thickness parameters mainly affect structural mass with comparatively limited impact on dynamic accuracy. Accordingly, an optimization problem with 10 geometric design variables was formulated to minimize total structural mass while constraining printhead displacement in the X and Y directions to within 1mm under unfavorable operating conditions. The GA demonstrated stable convergence without premature stagnation. The optimal design achieved a structural mass of 359.67kg, representing a 63.09% reduction relative to the initial configuration, while maintaining maximum printhead displacement below 0.112mm in the X direction and 0.815mm in the Y direction, thereby satisfying all prescribed technical requirements. By incorporating time-dependent dynamic response into the optimization process, the proposed approach more realistically represents operational conditions compared with conventional static-based methods. The framework provides an effective strategy for the design of large-scale mechanical structures subjected to dynamic loading.

Despite the promising results obtained, several limitations of the present study should be acknowledged. First, the direct evaluation of flexible dynamic responses within the optimization loop remains computationally expensive, particularly when a large number of design iterations is required. Second, the current optimization model is formulated as a single-objective problem focused on structural weight minimization, with time-dependent printhead displacement considered as the primary design constraint. Third, the proposed methodology has been validated only through numerical simulations, and experimental verification of printhead displacement and structural vibration has not yet been conducted. Future work will therefore focus on extending the framework toward multi-objective and multi-constraint optimization, while incorporating surrogate models such as artificial neural networks (ANNs) to reduce computational cost. In addition, experimental studies, potentially using a scaled prototype, will be performed to further validate the proposed methodology and optimization results.

REFERENCES

[1]. Buswell R. A., Leal de Silva W. R., Jones S. Z., Dirrenberger J., "3D printing using concrete extrusion: A roadmap for research," *Cement and Concrete Research*, 112, 37-49, 2018.

[2]. Záda V., Belda K., "Structure Design and Solution of Kinematics of Robot Manipulator for 3D Concrete Printing," *IEEE Transactions on Automation Science and Engineering,* 19(4), 3723-3734, 2022.

[3]. Jo J. H., Jo B. W., Cho W., Kim J. H., "Development of a 3D Printer for Concrete Structures: Laboratory Testing of Cementitious Materials," *International Journal of Concrete Structures and Materials,* 14(1), 13, 2020.

[4]. Bos F., Wolfs R., Ahmed Z., Salet T., "Additive manufacturing of concrete in construction: potentials and challenges of 3D concrete printing," *Virtual and Physical Prototyping,* 11(3), 209-225, 2016.

[5]. Hai T. D., Binh P. V., Tung P. D., "Application of ANN and nature-inspired algorithm in design optimization of the frame of a large-scale 3D concrete printer," *Journal of Science and Technique,* 19(02), 2024. DOI: 10.56651/lqdtu.jst.v19.n02.717 (in Vietnamese).

[6]. Liu S., Du Y., Lin M., "Study on lightweight structural optimization design system for gantry machine tool," *Concurrent Engineering,* 27(2), 170-185, 2019.

[7]. Besharati S., Dabbagh V., Amini H., Sarhan A., Akbari J., Abd Shukor M., Ong Z., "Multi-objective selection and structural optimization of the gantry in a gantry machine tool for improving static, dynamic, and weight and cost performance," *Concurrent Engineering,* 24, 2015.

[8]. Dang H. M., Bui V. P., Phung V. B., Thom D. V., Van Minh P., Gavriushin S. S., Duc N. V., "Development of a Generalized Mathematical Model for Slider-Crank Mechanism Based on Multiobjective Concurrent Engineering with Application," *Arabian Journal for Science and Engineering, 46*(8), 8037-8053, 2021.

[9]. Nguyen A. T., Han J. H., "Wing flexibility effects on the flight performance of an insect-like flapping-wing micro-air vehicle," *Aerospace Science and Technology,* 79, 468-481, 2018.

[10]. Nguyen A. T., Le V. D. T., Tran T. H., Duc V. N., Phung V. B., "Study of vertically ascending flight of a hawkmoth model," *Acta Mechanica Sinica*, 36(5), 1031-1045, 2020.

[11]. Ta Duc Hai, Nguyen Ba Thong, Nguyen Ngoc Binh, Phung Van Binh, "Application of artificial neural network (ANN) to calculate 3D concrete printer large-sized," *Journal of Science and Technology, Hanoi University of Industry, 60, 1*, 2024 DOI: http://doi.org/10.57001/huih5804.2024.034 (in Vietnamese).

[12]. Trieu D. K., Nguyen A. T., Ta D. H., Akoto R. A., "Development of an automatic program for dynamics analysis of 3D concrete printer frame with flexible links," *Journal of Science and Technique,* 20(02), 2025. DOI: 10.56651/lqdtu.jst.v20.n02.931.